Journal of Advanced Ceramics
2019, **8**(3): 367–376
https://doi.org/10.1007/s40145-019-0318-4
ISSN 2226-4108
CN 10-1154/TQ

Research Article

Slip casting and pressureless sintering of Ti_3AlC_2

Yimin GONG[a], Wubian TIAN[a,*], Peigen ZHANG[a], Jian CHEN[a], Yamei ZHANG[b], Zhengming SUN[a,*]

[a]*Jiangsu Key Laboratory of Advanced Metallic Materials, School of Materials Science and Engineering, Southeast University, Nanjing 211189, China*
[b]*Jiangsu Key Laboratory of Construction Materials, School of Materials Science and Engineering, Southeast University, Nanjing 211189, China*

Received: November 2, 2018; Revised: January 15, 2019; Accepted: January 24, 2019

Abstract: Slip casting and subsequent pressureless sintering (PLS) allow the preparation of complex-shaped and large-sized Ti_3AlC_2 components for many potential applications. The behaviors of the suspensions, green compacts, and sintered samples of Ti_3AlC_2 were studied in this paper. The optimized condition of 1 wt% of arabic gum as dispersant at pH = 10 results in a Ti_3AlC_2 suspension for slip casting Ti_3AlC_2 green compacts without macro defects or cracks. The sintering temperature and Al_4C_3 embedding powder are found to dominate the properties of the sintered Ti_3AlC_2 samples. The Ti_3AlC_2 sample sintered at 1450 ℃ for 1.5 h with Al_4C_3 embedding powder reaches the best properties, namely 95.3% relative density, hardness of 4.18 GPa, thermal conductivity of 29.11 $W \cdot m^{-1} \cdot K^{-1}$, and electrical resistivity of 0.39 μΩ·m. The findings in this work may pave the way for the application of MAX phases with large size and complex shape.

Keywords: slip casting; pressureless sintering (PLS); properties; Ti_3AlC_2

1 Introduction

MAX phases, where M is a transition metal, A is a group A element, and X is either C or N, are a group of intriguing new materials [1]. Titanium aluminum carbide (Ti_3AlC_2), as a member of MAX family, possesses a combination of properties of metals and ceramics [2,3], such as low density (4.25 g/cm^3) [4], high electrical conductivity (0.23–0.35 μΩ·m) [5,6], high thermal shock resistance [4,7], low hardness (3.5 GPa) [6], low frictional coefficient [8], good machinability [9], excellent corrosion [10], and oxidation resistance up to 1000 ℃ [11,12]. Therefore, Ti_3AlC_2 is a promising candidate for high-temperature oxidation resistant components and friction materials, such as engines parts and sliding current collectors.

Dense bulk Ti_3AlC_2 materials are usually prepared by hot pressing (HP), hot isostatic pressing (HIP), or spark plasma sintering (SPS). Wang and Zhou [13,14] fabricated Ti_3AlC_2 compacts by HP at 1500 ℃ under 25 MPa for 5 min and subsequent annealing at 1200 ℃ for 20 min. Tzenov and Barsoum [4] prepared Ti_3AlC_2 compacts by HIP at 1400 ℃ under 70 MPa for 16 h. Zhou *et al.* [15] prepared Ti_3AlC_2 compacts by SPS at 1200–1250 ℃ under 30 MPa. These methods are mainly applied in laboratories due to the high sintering pressure and expensive facilities.

* Corresponding authors.
E-mail: W. Tian, wbtian@seu.edu.cn;
Z. Sun, zmsun@seu.edu.cn

In contrast to the aforementioned methods, pressureless sintering is more attractive for its high shape-forming flexibility and low cost. Li *et al.* [16] firstly reported the PLS of Ti_3SiC_2-based compacts from the mechanical alloyed Ti, Si, and C powders after die-pressing at 130–150 MPa and subsequent cold-isostatically pressing (CIP) at 200 MPa. In addition, colloidal processing routes, such as tape casting and slip casting in a strong magnetic field, were utilized to fabricate MAX phase compacts (Nb_4AlC_3 and Ti_3SiC_2) with oriented microstructure [16–18].

Slip casting and pressureless sintering provide an inexpensive processing to fabricate complex-shaped and large-sized ceramic components [19,20]. As far as we know, however, there are only two reports in the literature on the slip casting or PLS of Ti_3AlC_2. Sun *et al.* [21] have explored the slip casting of Ti_3AlC_2 slurries. The authors focused on the effect of surface hydroxyl groups on slurry stability, such as≡Ti –OH, ＝Al–OH, and －OTi–$(OH)_2$, but the sinterability of Ti_3AlC_2 was not reported. Lu and Zhou [22] have fabricated bulk Ti_3AlC_2 by cold-isostatically pressing (CIP) under 200 MPa and PLS with different embedding powders like Si, Ti_3AlC_2, and Al_4C_3. Ti_3AlC_2 compacts embedded in Al_4C_3 powder pressurelessly sintered at 1450 ℃ for 150 min reached the highest 96.2% relative density.

Generally, high forming or sintering pressure was necessary to densify the MAX samples, which limits the size and shape of parts produced [22]. In this article, therefore, the ultimate objective was to demonstrate the possibility of fabricating Ti_3AlC_2 by using slip casting and pressureless sintering. Firstly, Ti_3AlC_2 slurries were prepared based on a balance between the viscosity and zeta potential results. Then, the slip casting of Ti_3AlC_2 slurries was conducted to prepare green compacts and the pressureless sintering was carried out to fabricate dense Ti_3AlC_2 samples. Finally, the mechanical, thermal, and electrical properties of the fabricated Ti_3AlC_2 sample were examined.

2 Experimental

2. 1 Synthesis of Ti_3AlC_2 powder

TiC (2–4 μm, 99%), Ti (< 300 mesh, 99.99%), and Al (< 300 mesh, 99.7%) were used as starting materials. Ti_3AlC_2 powder was synthesized from TiC:Ti:Al with a molar ratio of 1.8:1:1 at 1450 ℃ for 2 h. The phase content of Ti_3AlC_2 powder was identified by an XRD equipment (D8-Discover, Bruker Co., Germany), using Cu Kα radiation at a scanning rate of 5 (°)/min. The particle size and microstructure of Ti_3AlC_2 powder were measured by a laser particle size analyzer (Microtrac S3500, Microtrac Inc., America) and scanning electron microscope (SEM, Sirion, FEI Co., America), respectively.

2. 2 Preparation of Ti_3AlC_2 suspension

For comparison, arabic gum (powder, Alading Chemical Industry Ltd., China) and polyacrylic acid (PAA, 50 wt% aqueous solution, Alading Chemical Industry Ltd., China) with an average molecular weight of 3000 g/mol were used as dispersants in preparing Ti_3AlC_2 suspension.

The Ti_3AlC_2 suspensions consisted of the as-prepared Ti_3AlC_2 powder, the desired dispersant, and the deionized water. The suspensions had a 50 wt% solid content. The pH value of the suspensions was adjusted by dripping hydrochloric acid (HCl) or ammonium hydroxide (NH_4OH). The suspensions were mixed with a planet ball-milling machine (QM-QX, Nanjing Instrument Co., Ltd., China) at a rate of 50 Hz for 4 h.

2. 3 Viscosity and zeta-potential measurements

The viscosity of the prepared suspensions was measured with a viscometer (NDJ-5S, Lichen Technology Inc., China) at a rotate speed of 60 r/min at 20 ℃. Zeta-potential measurements were performed with a zeta potentiometer (Zetasizer Nano, Malvern Instruments Ltd., England) for the 4 wt% Ti_3AlC_2 suspensions. The zeta potentials, representing the dispersity of suspensions, were recorded as a function of the pH of the suspension.

2. 4 Slip casting of Ti_3AlC_2 suspension

The Ti_3AlC_2 suspensions were poured into gypsum molds with a diameter of 25 mm. After consolidated at room temperature for 24 h, the green compacts were dried at 80 ℃ for 24 h. The macrophotographs of the green compacts were observed to show their integrity. The densities of green compacts were simply calculated by dividing mass with volume.

2. 5 PLS of Ti_3AlC_2 green compacts

Ti_3AlC_2 green compacts were dwelled at 300 ℃ for 2 h to degrease the dispersant, and then pressureless sintered at 1350–1500 ℃ for 1.5 h in a flowing Ar atmosphere

at a heating rate of 3 ℃/min. For comparison, the green compacts were sintered with or without Al_4C_3 embedding powders.

2. 6 Characterization of the sintered Ti_3AlC_2

The diametral shrinkage of the sintered Ti_3AlC_2 samples was measured with Vernier caliper and compared with green compacts. The density of sintered samples was measured using Archimedes method. Phase identification was conducted via X-ray diffraction (XRD).

The Vickers hardness was measured under a load of 10 N for 15 s. Specimens with dimensions of Φ12.7 mm × 3 mm were used for thermal conductivity measurements (LFA467, NETZSCH Co., Germany). The electrical resistivity was measured with a multimeter (METRAHIT 27I, Gossen-Metrawatt Co., Germany). The fracture surfaces of the bulk samples were observed by SEM equipped with an energy-dispersive spectroscopy (EDS) system.

3 Results and discussion

3. 1 Characteristic of the synthesized Ti_3AlC_2 powder

Figure 1 shows the XRD pattern of Ti_3AlC_2 powders synthesized from TiC, Ti, and Al mixture at 1450 ℃ for 2 h in flowing Ar. The peaks could be entirely indexed to Ti_3AlC_2 and TiC phases. The contents of the Ti_3AlC_2 and TiC phases can be quantitatively estimated from the integrated XRD peak intensities according to following equations [23]:

$$W_{\mathrm{TAC}} = \frac{I_{\mathrm{TAC}}}{I_{\mathrm{TAC}} + 0.084 I_{\mathrm{TC}}} \quad (1)$$

$$W_{\mathrm{TC}} = \frac{I_{\mathrm{TC}}}{11.905 I_{\mathrm{TAC}} + I_{\mathrm{TC}}} \quad (2)$$

where W_{TAC} and W_{TC} are the mass fraction of Ti_3AlC_2 and TiC, respectively. I_{TAC} and I_{TC} are the integrated peak intensity of Ti_3AlC_2 (002) and TiC (111), respectively. Accordingly, the purity of the synthesized Ti_3AlC_2 powders is determined to be 99.7%.

Figure 2 shows the particle size distribution of Ti_3AlC_2 powders after crushing and screening with 120 mesh. The cumulative volume of D_{10}–D_{90} for Ti_3AlC_2 particle is from 1.98 to 23.13 μm, and D_{50} of Ti_3AlC_2 powders is 8.35 μm.

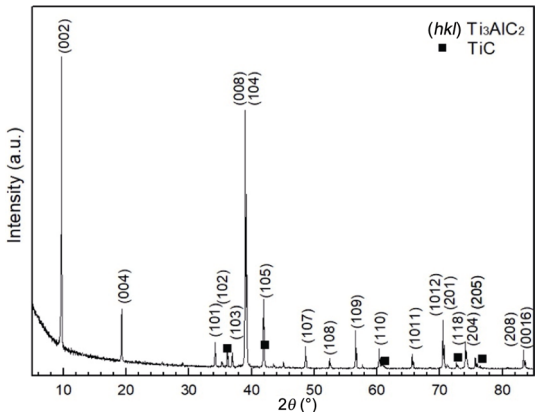

Fig. 1 XRD pattern of Ti_3AlC_2 powders synthesized from TiC, Ti, and Al mixture at 1450 ℃ for 2 h in flowing Ar.

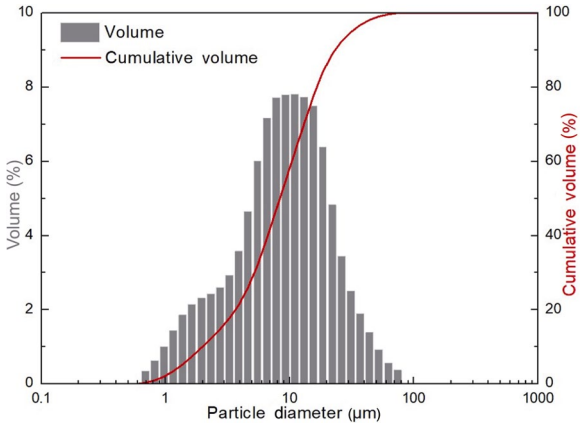

Fig. 2 Particle size distribution of Ti_3AlC_2 powders after screening.

3. 2 Properties of the Ti_3AlC_2 suspensions and the green compacts

The preparation of well dispersed and stabilized suspensions is the prerequisite to achieve high density and sound properties of the sintered samples [24,25]. Table 1 shows the label, dispersant type, mass fraction, pH of Ti_3AlC_2 suspensions as well as the relative density of Ti_3AlC_2 green compacts. The label of batches was identified as follows: the number before the letter means the mass fraction of dispersant; the letter means the type of dispersant (A: arabic gum; P: PAA); and the number after the letter means the pH of suspensions.

The viscosity of the Ti_3AlC_2 suspensions is an important indication of their capacity to yield intact green compacts. Figure 3 shows the dependence of viscosity on the pH value for the Ti_3AlC_2 suspensions listed in Table 1. For the Ti_3AlC_2 suspensions without

Table 1 Label, dispersant type, mass fraction, pH of Ti_3AlC_2 suspensions as well as the relative density of Ti_3AlC_2 green compacts

No.	Mass fraction of dispersant (wt%)	Dispersant	pH	Relative density of green compact (%)
1A4	1	Arabic gum	4	47.17
1A6	1	Arabic gum	6	45.14
1A8	1	Arabic gum	8	45.19
1A9	1	Arabic gum	9	45.89
1A10	1	Arabic gum	10	37.56
1A12	1	Arabic gum	12	37.50
2A4	2	Arabic gum	4	44.29
2A6	2	Arabic gum	6	46.23
2A8	2	Arabic gum	8	45.19
2A9	2	Arabic gum	9	37.72
2A10	2	Arabic gum	10	36.66
2A12	2	Arabic gum	12	45.61
1P4	1	Polyacrylic acid	4	44.09
1P5	1	Polyacrylic acid	5	38.68
1P6	1	Polyacrylic acid	6	37.48
1P7	1	Polyacrylic acid	7	43.56
2P4	2	Polyacrylic acid	4	38.89
2P5	2	Polyacrylic acid	5	37.74
2P6	2	Polyacrylic acid	6	40.35
2P7	2	Polyacrylic acid	7	37.93

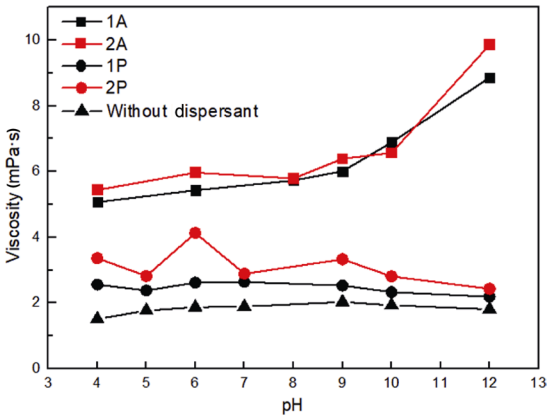

Fig. 3 Dependence of viscosity on the pH value for the Ti_3AlC_2 suspensions with Arabic gum and PAA dispersants.

dispersant, the pH has little effect on the viscosity. The viscosity stabilizes around 1.5 mPa·s. For PAA, the pH has little effect on the viscosity. The dispersant amount shows slightly influence on the viscosity. For arabic gum, the viscosity increases from 5 to 7 mPa·s as pH changes from 4 to 10, while rises to 9 mPa·s at pH of 12. Omura *et al.* [26] have found that the Al_2O_3 suspensions with a viscosity of 6 mPa·s is available for slip casting. In the aspect of viscosity results, arabic gum at pH around 10 could be the best choice for the slip casting of Ti_3AlC_2. Actually, the slip-casted 1A10 and 2A10 green compacts show the relatively intact shape if compared with other samples (Fig. 4).

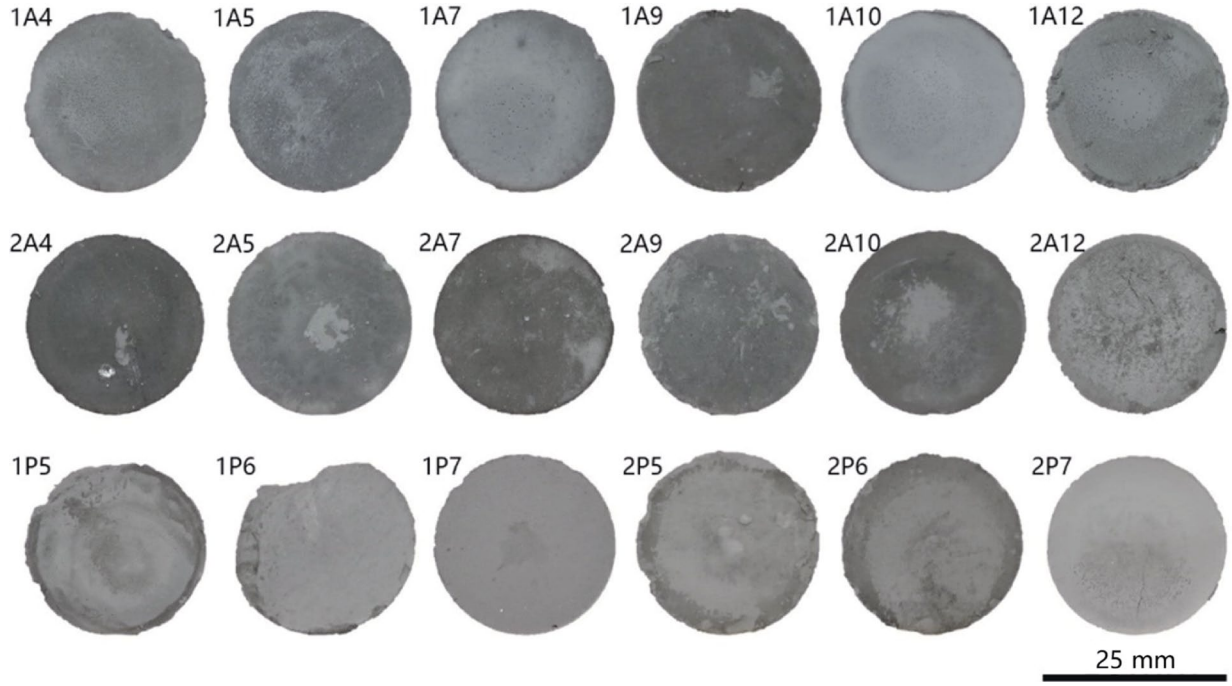

Fig. 4 Front view photographs of slip-casted Ti_3AlC_2 green compacts.

Van der Waals force in suspension results in the agglomeration of colloidal particles, and electrostatic repulsive forces must be introduced into the system to stabilize suspension. The electrostatic repulsion can be identified by zeta potential and adjusted by pH of suspension, as explained by the DLVO theory [27]. The pH dependence of the zeta potential in water solutions of Ti_3AlC_2 is shown in Fig. 5. For the Ti_3AlC_2 suspensions without dispersant, the absolute value of zeta potential stabilizes around 20 mV, and the maximum absolute value was 28.7 mV at pH = 10. For PAA dispersant, the zeta potential changes slightly with pH and the maximum absolute value was 43.1 mV at pH = 10 with the addition of 1wt% dispersant. For arabic gum dispersant, the zeta potential varies significantly and the maximum absolute value was 57.7 mV at pH = 10 with the addition of 1wt% dispersant. The dispersant amount has slight influence on the zeta potential of suspensions. Hunter [28] mentioned that the higher zeta potential absolute value leads to the more stable suspension. Therefore, in the aspect of zeta potential, arabic gum is more available than PAA as a dispersant of Ti_3AlC_2 suspension.

The effect of colloidal properties upon the slip casting behavior of a suspension has been described in terms of filtration theory [20]. Figure 4 shows the photographs of Ti_3AlC_2 green compacts after slip casting. Ti_3AlC_2 green compacts with arabic gum dispersant maintain better integration than the ones with PAA dispersant. This accords with the above viscosity and zeta potential results. Especially, the 1A10 compact shows the most integrate shape, which is utilized to fabricate bulk Ti_3AlC_2 sample. The relative densities of these samples are shown in Table 1, ranging from 36.66% to 47.17%.

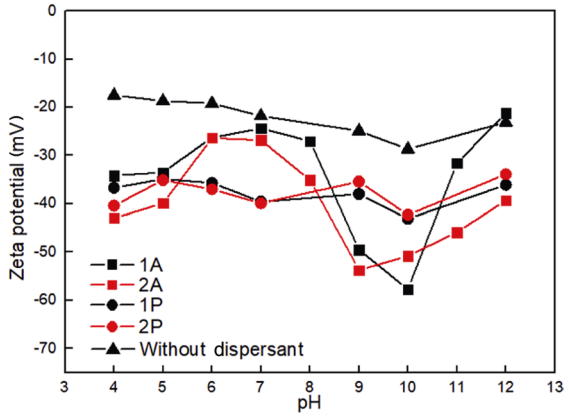

Fig. 5 Dependence of zeta potential on the pH value in the suspensions of Ti_3AlC_2 powder with arabic gum or PAA as dispersant.

3. 3 Properties of the sintered Ti_3AlC_2 samples

The effects of sintering temperature and embedding powder on the densification of the Ti_3AlC_2 green compact were explored to optimize the pressureless sintering process. Based on the analysis of dispersion properties, the most integrate sample 1A10 was sintered from 1350 to 1500 ℃ for 1.5 h in argon at a heating rate of 3 ℃/min. Figure 6 shows the optical photographs of the 1A10 green compacts and the samples sintered at 1350, 1400, 1450, and 1500 ℃ successively with and without embedding Al_4C_3 powder.

The Ti_3AlC_2 samples sintered at temperatures under 1450 ℃ show integrate shapes after sintering (Figs. 6(a) and 6(b)). Whereas, there are many particles on the surface (Fig. 6(a)) and cracks or macro deformation (Fig. 6(b)) for the Ti_3AlC_2 samples sintered at 1500 ℃. Therefore, the sintering temperature of 1500 ℃ is not available for the densification of Ti_3AlC_2 samples.

The linear shrinkage of sintered Ti_3AlC_2 sample can be calculated by the following equation:

$$\eta = \frac{l_0 - l}{l_0} \times 100\% \tag{3}$$

where l_0 and l are the diameters of the sample before and after sintering, respectively.

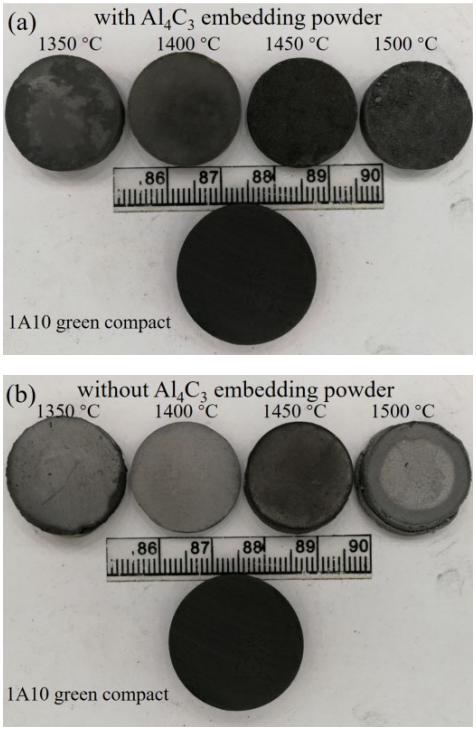

Fig. 6 1A10 green compacts and sintered samples (a) with and (b) without Al_4C_3 embedding powders ranging from 1350 to 1500 ℃.

The relationship between the linear shrinkage and the sintering temperature of the sintered Ti_3AlC_2 samples is shown in Fig. 7. The linear shrinkage increases with the sintering temperature at temperatures lower than 1450 ℃ and then decreases at higher temperatures. Besides, the linear shrinkage of the samples sintered with embedding Al_4C_3 powders is higher than those sintered without Al_4C_3 powders, which means the embedding powders are in favor of the shrinkage of sintered mass. The maximum shrinkage value reaches 15.35% in the sample sintered at 1450 ℃ with Al_4C_3 embedding powders.

Figure 8 presents the XRD patterns of the synthesized Ti_3AlC_2 powders and sintered samples with or without embedding Al_4C_3 powders in the temperature range of 1350–1500 ℃. The peaks of sintered samples can be indexed as Ti_3AlC_2 phase and TiC phase. The intensity of TiC peaks changes slightly as sintered at 1350–1400 ℃ with or without embedding Al_4C_3 powders. At 1450 ℃, the intensity of TiC peak increases sharply, especially the sample sintered without embedding Al_4C_3 powders. However, when the sintering temperature reaches up to 1500 ℃, most of the Ti_3AlC_2 decomposes into TiC. Note that the strongest peak changes from Ti_3AlC_2 (002) in powder to Ti_3AlC_2 (104) [4] in PLSed samples (e.g., at 1400 ℃).

Table 2 shows the estimated Ti_3AlC_2 and TiC phase contents in the samples sintered at 1350–1500 ℃ for 1.5 h with or without Al_4C_3 embedding powders. The phase content of Ti_3AlC_2 sustains around 97% at temperatures below 1450 ℃ and decreases significantly to 35% at 1500 ℃ for the samples sintered with Al_4C_3 powders. Whereas, the Ti_3AlC_2 sample entirely

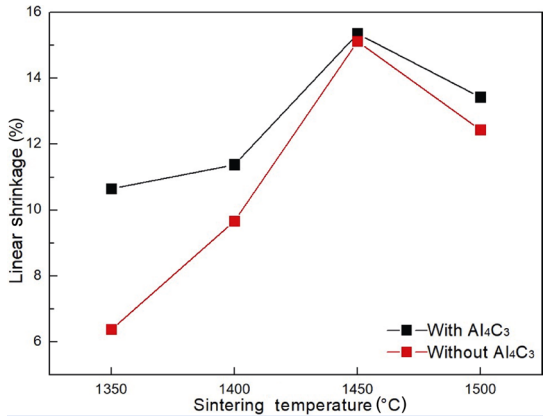

Fig. 7 Dependence of the linear shrinkage on the sintering temperature of Ti_3AlC_2 sample sintered with or without embedding Al_4C_3 powders.

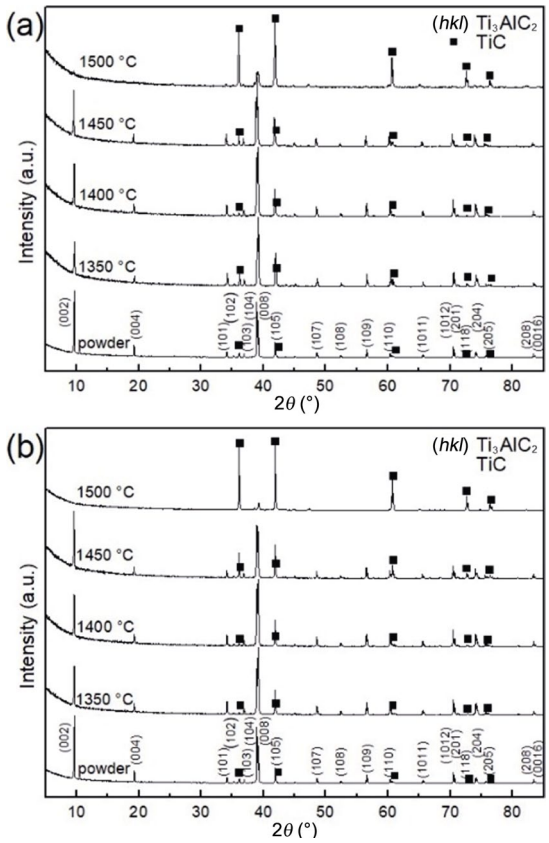

Fig. 8 XRD patterns of the samples 1A10 sintered at 1350–1500 ℃ for 1.5 h (a) with Al_4C_3 embedding powders and (b) without Al_4C_3 embedding powders.

Table 2 Estimated Ti_3AlC_2 and TiC contents in samples sintered at different temperatures with or without Al_4C_3 embedding powders (Unit: wt%)

	Phase	1350 ℃	1400 ℃	1450 ℃	1500 ℃
With Al_4C_3	Ti_3AlC_2	97.30	97.71	97.84	34.70
	TiC	2.70	2.29	2.16	65.30
Without Al_4C_3	Ti_3AlC_2	99.51	99.33	95.56	0
	TiC	0.49	0.67	4.04	100

decomposed as sintered at 1500 ℃ without embedding powders, indicating that Al_4C_3 powder inhibits the decomposition of Ti_3AlC_2 due to offering an Al-rich ambiance [22]. The Ti_3AlC_2 contents for the sintered samples (97.3%–99.5%) are slightly lower than that of the as-prepared powder (99.7%) for the decreased peak intensity of Ti_3AlC_2 (002). And the different Ti_3AlC_2 content for the samples sintered at temperatures below 1400 ℃ is probably related to the machining thickness for XRD tests.

3.4 Effects of sintering temperature and embedding powder on the properties of the sintered Ti_3AlC_2 samples

The theoretical density of the sintered 1A10 samples can be calculated with the following equation:

$$\rho = W_{TAC}\rho_{TAC} + W_{TC}\rho_{TC} \quad (4)$$

where W_{TAC} and W_{TC} are the mass percentage of Ti_3AlC_2 and TiC, respectively. As shown in Table 2, ρ_{TAC} and ρ_{TC} are the density of Ti_3AlC_2 (4.25 g/cm^3) and TiC (4.93 g/cm^3) [29], respectively. The ratio of the measured density to the theoretical density gives the relative density.

The relative density of the sintered 1A10 samples, taking both the content of Ti_3AlC_2 and TiC into consideration, is shown in Fig. 9. The variation tendency of the relative density accords with the linear shrinkage of sintered samples, as shown in Fig. 7. The relative density increases with the sintering temperature at temperatures lower than 1450 ℃ and then decreases at higher temperatures. Besides, the relative density of the samples sintered with embedding Al_4C_3 powders is higher than those sintered without Al_4C_3 powders. After sintered at 1450 ℃ for 1.5 h with Al_4C_3 embedding powders, the 1A10 sample has a measured density of 4.065 g/cm^3, corresponding to a maximum relative density of 95.32%. It shows that the embedding powders contribute to the densification of Ti_3AlC_2 sample, and the optimal sintering temperature is 1450 ℃.

Generally, the density of ceramic increases with sintering temperature. Whereas, Ti_3AlC_2 would decompose into TiC_x and Al at temperatures above 1400 ℃ due to the relatively weak metallic bond of Ti_{II}–Al [30,31]. The slight decomposition of Ti_3AlC_2 (1400–1450 ℃) promotes the densification of the samples for the presence of liquid or gaseous Al phase [32]. However, severe decomposition of Ti_3AlC_2 (1500 ℃) lowers the density due to the formation of large amount TiC_x and deficiency of Al. Al_4C_3 embedding powders can enhance the density of sintered samples because it provides Al-rich ambience that prohibits the diffusion of Al from Ti_3AlC_2.

Figures 10–12 show the Vickers hardness, thermal conductivity, and electrical resistivity of the prepared 1A10 samples. The Vickers hardness of 1A10 samples sintered with Al_4C_3 embedding powders increases linearly, reaching the peak value of 4.18±0.25 GPa at 1450 ℃, and decreases at 1500 ℃, as shown in Fig. 10. For 1A10 samples sintered without Al_4C_3 embedding powders, the Vickers hardness increases with sintering temperature and reaches the highest value of 4.81±0.25 GPa at 1500 ℃. Figure 11 shows the thermal conductivity that displays the highest value of 29.11 W·m^{-1}·K^{-1} as sintered at 1450 ℃ with Al_4C_3 embedding powders, which is fairly comparable to the value of 40 W·m^{-1}·K^{-1} of the hot-pressing sintered sample [33]. Figure 12 shows that the electrical resistivity reaches the minimum value 0.39 μΩ·m as sintered at 1450 ℃ with Al_4C_3 embedding powders, which is close to the reported value of 0.23–0.35 μΩ·m [5,6]. The variations of hardness, thermal conductivity, and electrical resistivity are attributed to the coupling effects of density and the decomposing product TiC.

Table 3 compares the properties of Ti_3AlC_2 samples prepared with HP, HIP, SPS, and PLS in this paper. The relative density of the PLSed Ti_3AlC_2 sample reaches 95.3%, which is close to the other samples. The PLSed Ti_3AlC_2 sample shows the highest purity and an

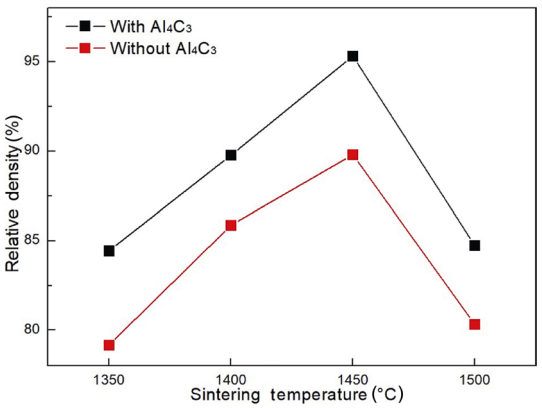

Fig. 9 Dependence of the relative density on the sintering temperature of Ti_3AlC_2 samples sintered with or without embedding Al_4C_3 powders.

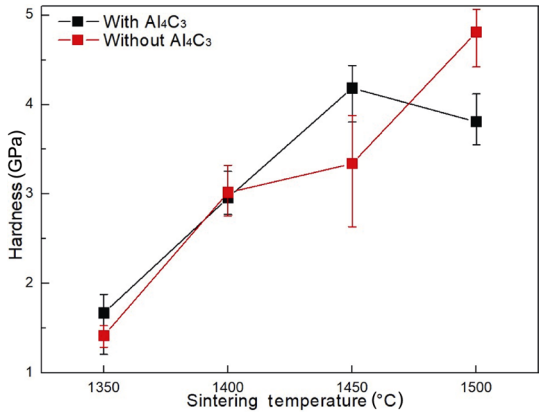

Fig. 10 Dependence of the Vickers hardness on the sintering temperature of Ti_3AlC_2 sample sintered with or without Al_4C_3 embedding powders.

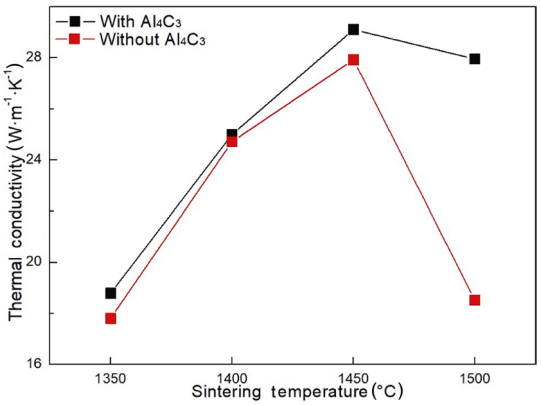

Fig. 11 Dependence of the thermal conductivity on the sintering temperature of Ti_3AlC_2 sample sintered with or without Al_4C_3 embedding powders.

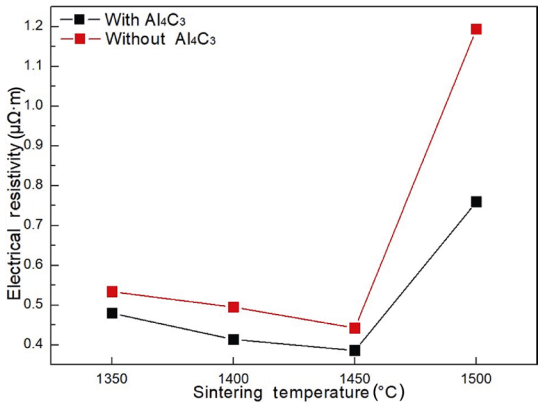

Fig. 12 Dependence of the electrical resistivity on the sintering temperature of Ti_3AlC_2 sample sintered with or without Al_4C_3 embedding powders.

Table 3 Comparison of the properties of Ti_3AlC_2 samples prepared by HP, HIP, SPS, and PLS

Method	Processing	Relative density (%)	Purity	*Hv* (GPa)	Ref.
HP	Ti, Al, and C HPed at 800 ℃ under 28 MPa	99	> 90 vol%	4.4	[33]
HIP	Ti, Al_4C_3, and C HIPed at 1400 ℃ under 70MPa for 16 h	—	96 vol%	3.5	[3]
SPS	Ti, Al, and C SPSed at 1450 ℃ under 20 MPa for 5 min	98.4	—	3.8	[34]
PLS	Slip casted Ti_3AlC_2 green compacts PLSed at 1450 ℃ with embedding Al_4C_3 for 1.5 h	95.3	97.84 wt%	4.18	This work

intermediate Vickers hardness. The utilization of slip casting and PLS technology in this paper testify the feasibility to prepare the complex-shaped and large-sized Ti_3AlC_2 components.

The typical SEM micrographs on the fracture surfaces of Ti_3AlC_2 sample sintered at 1450 ℃ with Al_4C_3 embedding powder were shown in Figs. 13(a) and 13(b). The Ti_3AlC_2 sample displays mainly intergranular fracture (Fig. 13(a)) and the layered grains (as indicated in Fig. 13(b)), in which small amount of pores exhibit. Figure 13(c) shows the elemental mapping of the same area in Fig. 13(b), demonstrating the uniform distribution of Ti, Al, and C elements. Besides, some portions are rich in Al and O elements but deficient in Ti and C (the arrow in Fig. 13(c)), which might result from the formation of Al_2O_3. The EDS result also confirms the presence of Ti_3AlC_2 and trace amount of Al_2O_3 (Fig. 13(d)).

4 Conclusions

The properties of the suspensions, green compacts, and sintered samples of Ti_3AlC_2 were studied. The main conclusions are as follows:

(1) The Ti_3AlC_2 suspension is stabilized by adding 1.0 wt% arabic gum at pH = 10, where the zeta potential reaches a maximum absolute value of 57.7 mV. Such prepared suspension leads to Ti_3AlC_2 green compact with the least defects.

(2) During the PLS of Ti_3AlC_2 compacts with Al_4C_3 embedding powders, the purity of Ti_3AlC_2 maintains up to 1450 ℃ and decreases at 1500 ℃. The relative density of Ti_3AlC_2 compacts reaches a maximum value of 95.3% at 1450 ℃.

(3) The Ti_3AlC_2 sample sintered at 1450 ℃ with Al_4C_3 embedding powders presents the optimum properties with a hardness of 4.18 GPa, a thermal conductivity of 29.11 $W \cdot m^{-1} \cdot K^{-1}$, and an electrical resistivity of 0.39 μΩ·m. These properties are quite close to the samples prepared by conventional pressure-assisted sintering methods.

Acknowledgements

This research was financially supported by National Natural Science Foundation of China (51731004, 51671054, 51501038), Natural Science Foundation of Jiangsu Province (BK20181285), and "the Fundamental Research Funds for the Central Universities" in China (2242018K40108, 2242018K40109).

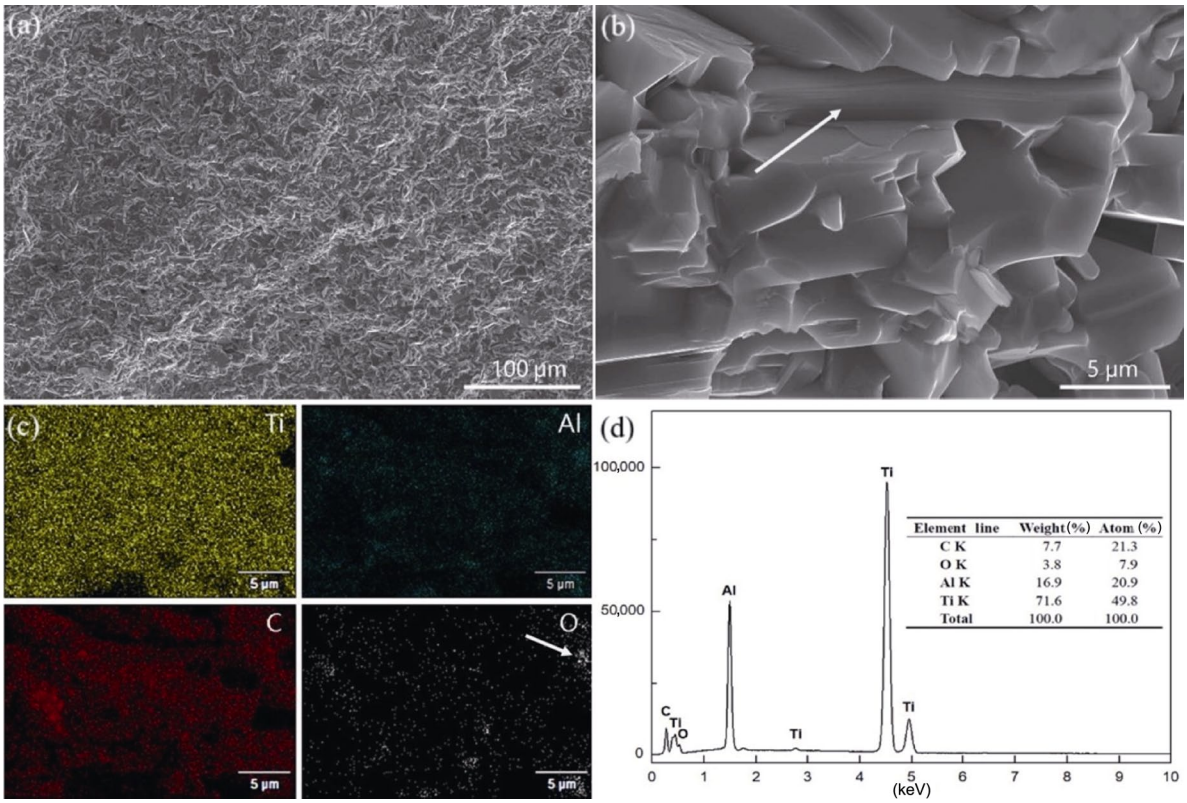

Fig. 13 (a, b) The typical SEM images on the fracture surfaces of Ti_3AlC_2 sample sintered at 1450 ℃ with Al_4C_3 embedding powder, (c) elemental mapping, and (d) EDS spectrum of the same area in (b).

References

[1] Barsoum MW. The $M_{N+1}AX_N$ phases: A new class of solids: Thermodynamically stable nanolaminates. *Prog Solid State Chem* 2000, **28**: 201–281.

[2] Sun ZM. Progress in research and development on MAX phases: A family of layered ternary compounds. *Int Mater Rev* 2011, **56**: 143–166.

[3] Xu LD, Zhu DG, Grasso S, *et al*. Effect of texture microstructure on tribological properties of tailored Ti_3AlC_2 ceramic. *J Adv Ceram* 2017, **6**: 120–128.

[4] Tzenov NV, Barsoum MW. Synthesis and characterization of Ti_3AlC_2. *J Am Ceram Soc* 2004, **83**: 825–832.

[5] Zou Y, Sun ZM, Tada S SJ, *et al*. Effect of liquid reaction on the synthesis of Ti_3SiC_2 powder. *Ceram Int* 2008, **34**: 119–123.

[6] Barsoum MW, Yoo HI, Polushina IK, *et al*. Electrical conductivity, thermopower, and hall effect of Ti_3AlC_2, Ti_4AlN_3, and Ti_3SiC_2. *Phys Rev B* 2000, **62**: 10194–10198.

[7] Bao YW, Wang XH, Zhang HB, *et al*. Thermal shock behavior of Ti_3AlC_2 from between 200 ℃ and 1300 ℃. *J Eur Ceram Soc* 2005, **25**: 3367–3374.

[8] Zhai HX, Huang ZY, Ai MX, *et al*. Tribophysical properties of polycrystalline bulk Ti_3AlC_2. *J Am Ceram Soc* 2005, **88**: 3270–3274.

[9] Bao YW, Chen JX, Wang XH, *et al*. Shear strength and shear failure of layered machinable Ti_3AlC_2 ceramics. *J Eur Ceram Soc* 2004, **24**: 855–860.

[10] Sun DD, Zhou AG, Li ZY, *et al*. Corrosion behavior of Ti_3AlC_2 in molten KOH at 700 ℃. *J Adv Ceram* 2013, **2**: 313–317.

[11] Tallman DJ, Anasori B, Barsoum MW. A critical review of the oxidation of Ti_2AlC, Ti_3AlC_2 and Cr_2AlC in air. *Mater Res Lett* 2013, **1**: 115–125.

[12] Wang XH, Zhou YC. Oxidation behavior of Ti_3AlC_2 at 1000–1400 ℃ in air. *Corros Sci* 2003, **45**: 891–907.

[13] Wang XH, Zhou YC. Solid–liquid reaction synthesis of layered machinable Ti_3AlC_2 ceramic. *J Mater Chem* 2002, **12**: 455–460.

[14] Wang XH, Zhou YC. Microstructure and properties of Ti_3AlC_2 prepared by the solid–liquid reaction synthesis and simultaneous *in situ* hot pressing process. *Acta Mater* 2002, **50**: 3143–3151.

[15] Zhou WB, Mei BC, Zhu JQ. Fabrication of high-purity ternary carbide Ti_3AlC_2 by spark plasma sintering (SPS) technique. *Ceram Int* 2007, **33**: 1399–1402.

[16] Li JF, Matsuki T, Watanabe R. Fabrication of highly dense Ti_3SiC_2 ceramics by pressureless sintering of mechanically alloyed elemental powders. *J Mater Sci* 2003, **38**: 2661–2666.

[17] Hu CF, Sakka Y, Tanaka H, *et al*. Fabrication of textured Nb_4AlC_3 ceramic by slip casting in a strong magnetic field and spark plasma sintering. *J Am Ceram Soc* 2011, **94**:

410–415.

[18] Sato K, Mishra M, Hirano H, *et al*. Fabrication of textured Ti_3SiC_2 ceramic by slip casting in a strong magnetic field and pressureless sintering. *J Ceram Soc Jpn* 2014, **122**: 817–821.

[19] Tiller FM, Tsai CD. Theory of filtration of ceramics: I, slip casting. *J Am Ceram Soc* 1986, **69**: 882–887.

[20] Lewis JA. Colloidal processing of ceramics. *J Am Ceram Soc* 2004, **83**: 2341–2359.

[21] Sun ZQ, Li MS, Hu LF, *et al*. Surface chemistry, dispersion behavior, and slip casting of Ti_3AlC_2 Suspensions. *J Am Ceram Soc* 2009, **92**: 1695–1702.

[22] Lu XP, Zhou YC. Pressureless sintering and properties of Ti_3AlC_2. *Int J Appl Ceram Technol* 2010, **7**: 744–751.

[23] Wang CA, Zhou AG, Qi L, *et al*. Quantitative phase analysis in the Ti–Al–C ternary system by X-ray diffraction. *Powder Diffr* 2005, **20**: 218–223.

[24] Michálek M, Bodišová K, Michálková M, *et al*. Alumina/MWCNTs composites by aqueous slip casting and pressureless sintering. *Ceram Int* 2013, **39**: 6543–6550.

[25] Zhang JX, Jiang DL, Tan SH, *et al*. Aqueous processing of titanium carbide green sheets. *J Am Ceram Soc* 2001, **84**: 2537–2541.

[26] Omura N, Hotta Y, Sato K, *et al*. Slip casting of Al_2O_3 slurries prepared by wet jet milling. *J Ceram Soc Jpn* 2005, **113**: 495–497.

[27] Derjaguin B, Landau L. Theory of the stability of strongly charged lyophobic sols and of the adhesion of strongly charged particles in solutions of electrolytes. *Prog Surf Sci* 1993, **43**: 30–59.

[28] Hunter RJ. The calculation of zeta potential. In *Zeta Potential in Colloid Science*. Elsevier, 1981: 59–124.

[29] Vallauri D, Atías Adrián IC, Chrysanthou A. TiC–TiB_2 composites: A review of phase relationships, processing and properties. *J Eur Ceram Soc* 2008, **28**: 1697–1713.

[30] Zhou YC, Sun ZM, Wang XH, *et al*. *Ab initio* geometry optimization and ground state properties of layered ternary carbides Ti_3MC_2(M = Al, Si and Ge). *J Phys: Condens Matter* 2001, **13**: 10001–10010.

[31] Pang WK, Low IM, Sun ZM. *In situ* high-temperature diffraction study of the thermal dissociation of Ti_3AlC_2 in vacuum. *J Am Ceram Soc* 2010, **93**: 2871–2876.

[32] Panigrahi BB, Gracio JJ, Chu MC, *et al*. Powder synthesis, sintering kinetics, and nickel-activated pressureless sintering of Ti_3AlC_2. *Int J Appl Ceram Technol* 2010, **7**: 752–759.

[33] Barsoum MW, Radovic M. Mechanical properties of the MAX phases. In *Encyclopedia of Materials: Science and Technology*, 2nd edn. Elsevier, 2004: 1–16.